

Fast Learnings of Coupled Nonnegative Tensor Decomposition Using Optimal Gradient and Low-rank Approximation

Xiulin Wang, Tapani Ristaniemi, *Senior Member, IEEE* and Fengyu Cong, *Senior Member, IEEE*

Abstract—Nonnegative tensor decomposition has been widely applied in signal processing and neuroscience, etc. When it comes to group analysis of multi-block tensors, traditional tensor decomposition is insufficient to utilize the shared/similar information among tensors. In this study, we propose a coupled nonnegative CANDECOMP/PARAFAC decomposition algorithm optimized by the alternating proximal gradient method (CoNCPD-APG), which is capable of a simultaneous decomposition of tensors from different samples that are partially linked and a simultaneous extraction of common components, individual components and core tensors. Due to the low optimization efficiency brought by the nonnegative constraint and the high-dimensional nature of the data, we further propose the lraCoNCPD-APG algorithm by combining low-rank approximation and the proposed CoNCPD-APG method. When processing multi-block large-scale tensors, the proposed lraCoNCPD-APG algorithm can greatly reduce the computational load without compromising the decomposition quality. Experiment results of coupled nonnegative tensor decomposition problems designed for synthetic data, real-world face image and event-related potential data demonstrate the practicability and superiority of the proposed algorithms.

Index Terms—Alternating proximal gradient, CANDECOMP/PARAFAC, coupled, low-rank approximation, nonnegative tensor decomposition

I. INTRODUCTION

DECOMPOSING a tensor into a minimal number of rank-1 tensors is known as CANDECOMP/PARAFAC (also known as Canonical Polyadic, [1, 2, 3]) decomposition (CPD). Nonnegative CPD (NCPD) provides a part-based representation of a tensor via imposing nonnegative constraints on its hidden factors, enabling us to extract more meaningful and convincing information [4]. For example, electroencephalography (EEG) data with spatial, temporal and subject features can be represented as a third-order tensor, and the underlying features can be simultaneously extracted through CPD [5].

Corresponding author: Fengyu Cong, email: cong@dlut.edu.cn

X. Wang and F. Cong are with the School of Biomedical Engineering, Faculty of Electronic Information and Electrical Engineering, Dalian University of Technology, Dalian 116024, China, and also with the Faculty of Information Technology, University of Jyväskylä, Jyväskylä 40100, Finland (e-mail: xiulin.wang@foxmail.com; cong@dlut.edu.cn). F. Cong is also with the School of Artificial Intelligence, Faculty of Electronic Information and Electrical Engineering, Dalian University of Technology, 116024, Dalian, China, and the Key Laboratory of Integrated Circuit and Biomedical Electronic System, Liaoning Province, Dalian University of Technology, 116024, Dalian, China. T. Ristaniemi is with the Faculty of Information Technology, University of Jyväskylä, Jyväskylä 40100, Finland (tapani.e.ristaniemi@jyu.fi).

Manuscript received Month Day, Year; revised Month Day, Year.

If time-frequency representation is further considered, non-negativity will naturally be brought into the EEG data, which should be solved by NCPD [6]. Although CPD/NCPD methods have received widespread attention both in theory and application, their main contribution lies in the decomposition analysis of a tensor represented by a single dataset [7, 8, 9]. Regarding emerging multi-block tensors (e.g., multi-subject/multi-modal biomedical data) that need to be analyzed together, traditional tensor decomposition methods become quite challenging in identifying and exploiting the connections between different tensors [10, 11]. For example, the internal sharing in EEG data of multiple subjects or the complementary spatiotemporal characteristics in the EEG-fMRI integrated data obviously cannot be effectively utilized in traditional methods [11, 12].

Coupled tensor decomposition, an extension of tensor decomposition to multi-block tensors, provides a natural solution for jointly analyzing two or more tensors [10, 13, 14]. Interestingly, the uniqueness condition for coupled tensor decomposition is more relaxed than that of single tensor decomposition [14, 15]. It can also take full advantage of the constraints (e.g., sparsity, smoothness and nonnegativity) so that it can obtain more unique solutions and interpretable components [16, 17]. Coupled tensor decomposition can achieve higher decomposition accuracy and stronger robustness, reveal the inner-relationships among tensor data, and maintain the potential interactions among multi-way structure of tensor data [5, 11, 16]. The interactions will inevitably be lost in two-way matrix counterparts [18, 19], and coupled tensor methods can circumvent the independent constraint [15, 20]. Moreover, coupled tensor decomposition of multi-block tensors can achieve the simultaneous extraction of common components shared by all blocks and individual components corresponding to individual block [21, 22, 23].

To date, increasing recognition of joint tensor analysis has led to the consideration of coupled tensor decomposition in a number of applications. In special cases, coupled matrix and tensor factorization (CMTF [24]) and its variants, including advanced CMTF [25] and coupled tensor-tensor decomposition (CTTD [12, 26]) have proved their superiority over ICA-based two-way methods in EEG and fMRI data fusion. The algebraic double coupled CPD (DC-CPD) algorithm using second-order statistics in joint blind source separation (JBSS) problem exhibits more relaxed uniqueness and higher accuracy than the standard CPD [13]. Linked CPD model optimized by hierarchical alternating least squares (HALS), fast HALS and alternating direction method of multipliers (ADMM) has also

achieved good performance in classification, image processing and biomedical signal processing [11, 21, 27, 28]. Common and individual feature extraction (CIFE) framework for multi-block data enables the separate extraction of common and individual components by incorporating dimensionality reduction and blind source separation (BSS) methods, and has been successfully applied to classification, clustering and linked BSS problems [10, 23]. Last but not the least, coupled tensor decomposition is also applied to data fusion of low spatial resolution hyperspectral (LRHS) and high spatial resolution multispectral (HRMS) images [29, 30], array signal processing [31], linked prediction[32] and metabolic physiology [33].

However, due to the nonnegative constraint and high-dimensional nature of tensor data, existing coupled tensor decomposition methods often suffer from slow convergence speed and low optimization accuracy [34, 35]. Therefore, aiming to effectively and efficiently achieve the joint analysis of tensors with coupled information, we propose two advanced coupled NCPD methods: coupled nonnegative CAN-DECOMP/PARAFAC decomposition algorithm based on alternating proximal gradient (CoNCPD-APG) and its fast implementation based on low-rank approximation (IraCoNCPD-APG). Specifically, our contributions in this study are listed as follows.

(1) Using the optimal gradient method, we propose an effective CoNCPD-APG algorithm for the joint analysis of multi-block tensors that are partially linked. It can realize the simultaneous decomposition of tensors with excellent decomposition accuracy.

(2) By introducing low-rank approximation, we further proposed an efficient IarCoNCPD-APG algorithm, which can greatly reduce the time consumption without losing the decomposition accuracy.

(3) The designed experiments on synthetic data, real-world face image and EEG data prove the practicability and superiority of the proposed algorithms.

The rest of this paper is organized as follows. Section II introduces some basic preliminaries and related work. In Section III, we present the proposed algorithms as well as some theoretical analyses. Experiments on synthetic and real-world data are designed in Section IV to verify the performance of the proposed algorithms. The last section concludes this paper.

II. PRELIMINARIES AND RELATED WORK

A. Notations and tensor operations

Tensor, also known as multi-way array, is the high-order generalization of vector and matrix. The order of a tensor is the number of dimensions, ways or modes of it. Generally, tensors are denoted by calligraphic boldface uppercase letters, matrices by boldface uppercase letters, vectors by boldface uppercase letters, and scalars by lowercase letters. Table I gives a summary of basic notations and mathematical operations throughout this study, and please refer to [7] for a more detailed description of them.

B. Optimal gradient method

Accelerated/Alternating proximal gradient (APG), an accelerated version of proximal gradient (PG, [36]), was orig-

TABLE I
BASIC NOTATIONS AND MATHEMATICAL OPERATIONS

Symbol	Definition
\mathbb{R}, \mathbb{R}_+	real number, nonnegative real number
\circ, \odot	outer product, Khatri-Rao product
\otimes, \oslash	element-wise (Hadamard) product, division
$(\cdot)^T, \text{vec}(\cdot)$	transpose, vectorization operator
$\llbracket \cdot \rrbracket, \langle \cdot, \cdot \rangle, \ \cdot\ _F$	Kruskal operator, inner product and Frobenius norm
$m, \mathbf{m}, \mathbf{M}, \mathcal{M}$	scalar, vector, matrix and tensor
$\mathcal{M}^{(n)}$	mode- n matricization of tensor \mathcal{M}
$\text{vec}(\mathcal{M})$	vectorization of tensor \mathcal{M}
$\text{ddiag}(\mathcal{M})$	vectorization of super-diagonal elements of tensor \mathcal{M}
$\text{ddiag}(\mathbf{m})$	tensorization with \mathbf{m} on the super-diagonal elements
$U_{i:j,:}$	row-wise submatrix of U , i th to j th row
$U_{:,i:j}$	column-wise submatrix of U , i th to j th column
$U^{(n)}$	the n -th factor matrix
${}^1 U^{\odot}$	$U^{(N)} \odot U^{(N-1)} \odot \dots \odot U^{(2)} \dots \odot U^{(1)}$
${}^2 U^{\odot-n}$	$U^{(N)} \odot \dots \odot U^{(n+1)} \odot U^{(n-1)} \dots \odot U^{(1)}$

^{1,2} U^{\otimes} and $U^{\otimes-n}$ are defined in the similar way.

inally proposed by Nesterov for smooth optimization with achieving the convergence rate of $\mathcal{O}(\frac{1}{K^2})$, where K is the number of iterations [37, 38]. For a minimization problem: $\min\{f(x), x \in \mathbb{R}^n\}$, assuming that $f(x) : \mathbb{R}^n \rightarrow \mathbb{R}$ is a convex function with Lipschitz continuous gradient f' , there will hold that

$$\|f'(x_i) - f'(x_j)\| \leq L \|x_i - x_j\|, \forall x_i, x_j \in \mathbb{R}^n \quad (1)$$

where $L > 0$ is the Lipschitz constant. To obtain an optimal point \tilde{x} , two sequences are updated successively in each iteration round (assume at the k th iteration) in APG method [37, 39] as follows:

$$x_k = \underset{x}{\text{argmin}} \left\{ \phi(x, x_{k-1}) = f(x_{k-1}) + \langle x - x_{k-1}, f'(x_{k-1}) \rangle + \frac{L}{2} \|x - x_{k-1}\|^2 \right\}, \quad (2)$$

and

$$x_{k+1} = x_k + \frac{\alpha_k - 1}{\alpha_{k+1}} (x_k - x_{k-1}) \quad (3)$$

with

$$\alpha_0 = 1, \alpha_{k+1} = \frac{1 + \sqrt{4\alpha_k^2 + 1}}{2} \quad (4)$$

where $\phi(x, x_{k-1})$ denotes the proximal regularized function of $f(x)$ at x_{k-1} and (3) denotes an extrapolated point by combining the points of current and previous iterations. Using the Lagrange multiplier method, from (2), we have

$$x_k \leftarrow \mathcal{P}(x_{k-1} - \frac{1}{L} f'(x_{k-1})) \quad (5)$$

where $\mathcal{P}(\cdot)$ denotes a shrinkage operator predefined by the user. Since each subproblem under block coordinate descent (BCD) framework is a convex function with Lipschitz continuous gradient, APG and its variants have proven to be very efficient for nonnegative matrix/tensor factorization issues and outperform many other competitors [35, 39, 40, 41, 42]. In the sequel, we adopt APG method to solve the coupled nonnegative tensor decomposition problems.

C. Coupled NCPD model

Given a set of N th-order nonnegative tensors $\mathcal{M}^{(s)} \in \mathbb{R}_+^{I_1 \times I_2 \times \dots \times I_N}$, $s = 1, 2, \dots, S$, the coupled NCPD model can be expressed as:

$$\begin{aligned} \mathcal{M}^{(s)} &\approx \hat{\mathcal{M}}^{(s)} = \sum_{r=1}^{R^{(s)}} \lambda_r^{(s)} \mathbf{u}_r^{(1,s)} \circ \mathbf{u}_r^{(2,s)} \circ \dots \circ \mathbf{u}_r^{(N,s)} \\ &= \left[\mathcal{D}^{(s)}; \mathbf{U}^{(1,s)}, \mathbf{U}^{(2,s)}, \dots, \mathbf{U}^{(N,s)} \right] \end{aligned} \quad (6)$$

where $\hat{\mathcal{M}}^{(s)} \in \mathbb{R}_+^{I_1 \times I_2 \times \dots \times I_N}$ denotes the estimated item of $\mathcal{M}^{(s)}$. $\mathbf{u}_r^{(n,s)} \in \mathbb{R}_+^{I_n}$ denotes the r th column of mode- n factor matrix of the s th tensor and $\mathbf{U}^{(n,s)} = \begin{bmatrix} \mathbf{u}_1^{(n,s)} & \mathbf{u}_2^{(n,s)} & \dots & \mathbf{u}_{R^{(s)}}^{(n,s)} \end{bmatrix} \in \mathbb{R}_+^{I_n \times R^{(s)}}$. $\mathcal{D}^{(s)} \in \mathbb{R}_+^{R^{(s)} \times \dots \times R^{(s)}}$ represents the s th core tensor with non-zero entries $\lambda_r^{(s)}$ only on its super-diagonal elements. $\hat{\mathcal{M}}_r^{(s)} = \lambda_r^{(s)} \mathbf{u}_r^{(1,s)} \circ \mathbf{u}_r^{(2,s)} \circ \dots \circ \mathbf{u}_r^{(N,s)}$ is termed as a rank-1 tensor generated by outer product of $\mathbf{u}_r^{(n,s)}$, $n = 1, 2, \dots, N$, and $\lambda_r^{(s)}$ is used to represent the scaling of rank-1 tensor. The decomposition of each tensor $\mathcal{M}^{(s)}$ can be regarded as decomposing a high-order tensor into a minimal number of rank-1 tensors, and the minimum number $R^{(s)}$ is termed as the rank of the tensor or the number of components.

In coupled NCPD model, we assume that each factor matrix includes two parts and satisfies $\mathbf{U}^{(n,s)} = \begin{bmatrix} \mathbf{U}_C^{(n,s)} & \mathbf{U}_I^{(n,s)} \end{bmatrix}$. $\mathbf{U}_C^{(n,s)} \in \mathbb{R}_+^{I_n \times L_n}$, $0 \leq L_n \leq \min(R^{(s)})$ represents the common information shared by all block-tensors as $\mathbf{U}_C^{(n,1)} = \dots = \mathbf{U}_C^{(n,S)} = \mathbf{U}_C^{(n)}$, and $\mathbf{U}_I^{(n,s)} \in \mathbb{R}_+^{I_n \times (R^{(s)} - L_n)}$ denotes the individual part corresponding to individual tensor. L_n represents the number of coupled components between tensors in the n th mode.

III. PROPOSED ALGORITHM

This section illustrates how to use APG method or combine APG method and low-rank approximation to solve the coupled NCPD problem. In addition, we give some discussions on the properties of the proposed algorithms as well as some implementation remarks.

A. Coupled NCPD using APG

For the coupled NCPD model, the optimization criterion of Euclidean divergence minimization is adopted to minimize the error between the original and estimated tensors. Therefore, given a set of nonnegative tensors $\mathcal{M}^{(s)}$, $s = 1, 2, \dots, S$, the objective function of coupled NCPD model can be presented as follows:

$$\begin{aligned} \min_{\mathcal{D}^{(s)}, \mathbf{U}^{(n,s)}} F &\frac{1}{2} \sum_{s=1}^S \left\| \mathcal{M}^{(s)} - \left[\mathcal{D}^{(s)}; \mathbf{U}^{(1,s)}, \dots, \mathbf{U}^{(N,s)} \right] \right\|_F^2 \\ \text{s.t., } \mathcal{D}^{(s)} &\in \mathbb{R}_+^{R^{(s)} \times \dots \times R^{(s)}}, \mathbf{U}^{(n,s)} \in \mathbb{R}_+^{I_n \times R^{(s)}} \end{aligned} \quad (7)$$

where $\mathbf{U}^{(n,s)} = \begin{bmatrix} \mathbf{U}_C^{(n,s)} & \mathbf{U}_I^{(n,s)} \end{bmatrix}$ and $\mathbf{U}_C^{(n,1)} = \dots = \mathbf{U}_C^{(n,S)} = \mathbf{U}_C^{(n)}$. According to BCD framework, the coupled NCPD

problem can be converted into several subproblems by optimizing $\mathcal{D}^{(s)}$ and $\mathbf{U}^{(n,s)}$ alternatively in each iteration. Each subproblem can be regarded as a minimization problem of a continuously differentiable function, which can be solved efficiently by APG method [39, 41, 42]. Next we provide a solution for coupled NCPD problem based on APG method.

First, regarding the solution of core tensor $\mathcal{D}^{(s)}$, we adopt (8) (see it at the top of next page). By keeping all the other variables and using the Lagrange multiplier method, $\mathcal{D}^{(s)}$ can be updated in a closed form as follows:

$$\mathcal{D}^{(s)} = \max \left(0, \hat{\mathcal{D}}^{(s)} - \frac{\hat{\mathcal{G}}^{(s)}}{L_d^{(s)}} \right) \quad (9)$$

where $\hat{\mathcal{D}}^{(s)}$ denotes an extrapolated point and $L_d^{(s)}$ denotes the Lipschitz constant of $F'(\mathcal{D}^{(s)})$. $\hat{\mathcal{G}}^{(s)}$ is the block-partial gradient of (7) at $\hat{\mathcal{D}}^{(s)}$, which can be calculated as:

$$\begin{aligned} \hat{\mathcal{G}}^{(s)} &= \text{ddiag} \left[\left(\mathbf{U}^{(s)T} \mathbf{U}^{(s)} \right)^{\otimes} \text{ddiag} \left(\hat{\mathcal{D}}^{(s)} \right) \right. \\ &\quad \left. - \left(\mathbf{U}^{(s)\odot} \right)^T \text{vec} \left(\mathcal{M}^{(s)} \right) \right] \end{aligned} \quad (10)$$

where $\text{vec}(\mathcal{M}^{(s)})$ denotes the vectorization of tensor $\mathcal{M}^{(s)}$. $\text{ddiag}(\mathcal{D}^{(s)})$ denotes a vector vectorized from the super-diagonal elements of $\mathcal{D}^{(s)}$, and the outer-loop notation $\text{ddiag}(\cdot)$ means the tensorization from a vector to a super-diagonal tensor, which is the reverse operation of the inner-loop $\text{ddiag}(\cdot)$.

Second, for the solution of factor matrix $\mathbf{U}^{(n,s)}$ (without coupled information), we adopt the updating method as (11) (see it at the top of next page), which can be written in the closed form as follows:

$$\mathbf{U}^{(n,s)} = \max \left(0, \hat{\mathbf{U}}^{(n,s)} - \frac{\hat{\mathbf{G}}^{(n,s)}}{L_u^{(n,s)}} \right) \quad (12)$$

where $\hat{\mathbf{U}}^{(n,s)}$ denotes an extrapolated point of $\mathbf{U}^{(n,s)}$, $L_u^{(n,s)}$ denotes a Lipschitz constant of block-partial gradient of (7) at $\mathbf{U}^{(n,s)}$. The block-partial gradient $\hat{\mathbf{G}}^{(n,s)}$ of (7) at $\hat{\mathbf{U}}^{(n,s)}$ is expressed as:

$$\begin{aligned} \hat{\mathbf{G}}^{(n,s)} &= \hat{\mathbf{U}}^{(n,s)} \mathcal{D}^{(s)} \left(\mathbf{U}^{(s)T} \mathbf{U}^{(s)} \right)^{\otimes -n} \mathcal{D}^{(s)} \\ &\quad - \mathcal{M}_{(n)}^{(s)} \mathbf{U}^{(s)\odot -n} \mathcal{D}^{(s)} \end{aligned} \quad (13)$$

where $\mathcal{M}_{(n)}^{(s)}$ denotes the mode- n matricization of $\mathcal{M}^{(s)}$. $\mathcal{D}^{(s)}$ is a diagonal matrix and its diagonal elements correspond to the super-diagonal elements of core tensor $\mathcal{D}^{(s)}$. However, for the factor matrix which includes $\mathbf{U}_C^{(n)}$ and $\mathbf{U}_I^{(n,s)}$, we need to calculate their solutions separately. Since $\mathbf{U}_C^{(n)}$ is shared by all tensors as $\mathbf{U}_C^{(n,1)} = \dots = \mathbf{U}_C^{(n,S)} = \mathbf{U}_C^{(n)}$, we should combine the information of all tensors to calculate the solution of $\mathbf{U}_C^{(n)}$. The solution of individual part $\mathbf{U}_I^{(n,s)}$ only needs to consider the corresponding s th-set tensor. Therefore, we have

$$\mathbf{U}_C^{(n)} = \max \left(0, \hat{\mathbf{U}}_C^{(n)} - \frac{\sum_{s=1}^S \hat{\mathbf{G}}_C^{(n,s)}}{\sum_{s=1}^S L_u^{(n,s)}} \right), \quad (14)$$

$$\mathcal{D}^{(s)} = \underset{\mathcal{D}^{(s)} \geq 0}{\operatorname{argmin}} \left[F(\hat{\mathcal{D}}^{(s)}) + \langle \hat{\mathcal{G}}^{(s)}, \mathcal{D}^{(s)} - \hat{\mathcal{D}}^{(s)} \rangle + \frac{L_d^{(s)}}{2} \left\| \mathcal{D}^{(s)} - \hat{\mathcal{D}}^{(s)} \right\|_F^2 \right] \quad (8)$$

$$\mathbf{U}^{(n,s)} = \underset{\mathbf{U}^{(n,s)} \geq 0}{\operatorname{argmin}} \sum_{s=1}^S \left[F(\hat{\mathbf{U}}^{(n,s)}) + \langle \hat{\mathbf{G}}^{(n,s)}, \mathbf{U}^{(n,s)} - \hat{\mathbf{U}}^{(n,s)} \rangle + \frac{L_u^{(n,s)}}{2} \left\| \mathbf{U}^{(n,s)} - \hat{\mathbf{U}}^{(n,s)} \right\|_F^2 \right] \quad (11)$$

and

$$\mathbf{U}_I^{(n,s)} = \max \left(0, \hat{\mathbf{U}}_I^{(n,s)} - \frac{\hat{\mathbf{G}}_I^{(n,s)}}{L_u^{(n,s)}} \right) \quad (15)$$

where $\hat{\mathbf{G}}_C^{(n,s)}$ and $\hat{\mathbf{G}}_I^{(n,s)}$ denote the block-partial gradients of (7) at $\hat{\mathbf{U}}_C^{(n,s)}$ and $\hat{\mathbf{U}}_I^{(n,s)}$, respectively. $\hat{\mathbf{U}}_C^{(n,s)}$ and $\hat{\mathbf{U}}_I^{(n,s)}$ denote the extrapolated points of $\mathbf{U}_C^{(n,s)}$ and $\mathbf{U}_I^{(n,s)}$. Moreover, $\hat{\mathbf{U}}^{(n,s)} = [\hat{\mathbf{U}}_C^{(n,s)} \ \hat{\mathbf{U}}_I^{(n,s)}]$ and $\hat{\mathbf{G}}^{(n,s)} = [\hat{\mathbf{G}}_C^{(n,s)} \ \hat{\mathbf{G}}_I^{(n,s)}]$.

Consider updating $\mathcal{D}^{(s)}$ and $\mathbf{U}^{(n,s)}$ at the k th iteration. The extrapolated points $\hat{\mathcal{D}}_{k-1}^{(s)}$ and $\hat{\mathbf{U}}_{k-1}^{(n,s)}$ are defined as

$$\hat{\mathcal{D}}_{k-1}^{(s)} = \mathcal{D}_{k-1}^{(s)} + w_{d,k-1}^{(s)} \left(\mathcal{D}_{k-1}^{(s)} - \mathcal{D}_{k-2}^{(s)} \right), \quad (16)$$

and

$$\hat{\mathbf{U}}_{k-1}^{(n,s)} = \mathbf{U}_{k-1}^{(n,s)} + w_{u,k-1}^{(n,s)} \left(\mathbf{U}_{k-1}^{(n,s)} - \mathbf{U}_{k-2}^{(n,s)} \right) \quad (17)$$

where $w_{d,k-1}^{(s)}$ and $w_{u,k-1}^{(n,s)}$ denote the extrapolation weights. Since APG is not a monotone method, i.e., $F(k)$ may not be smaller than $F(k-1)$. Therefore, if $F(k) \geq F(k-1)$ after iteration k , an additional re-updating of $\mathbf{U}_k^{(n,s)}$ and $\mathcal{D}_k^{(s)}$ will be taken via $\hat{\mathcal{D}}_{k-1}^{(s)} = \mathcal{D}_{k-1}^{(s)}$ and $\hat{\mathbf{U}}_{k-1}^{(n,s)} = \mathbf{U}_{k-1}^{(n,s)}$. In each iteration, we perform the optimization with the order $\mathcal{D}^{(1)}, \mathcal{D}^{(2)}, \dots, \mathcal{D}^{(S)}$ and $\mathbf{U}^{(1,1)}, \dots, \mathbf{U}^{(1,S)}, \dots, \mathbf{U}^{(N,1)}, \dots, \mathbf{U}^{(N,S)}$, which are alternatively updated one after another until convergence. We term the proposed coupled NCPD algorithm based on APG update as CoNCPD-APG and summarize it in Algorithm 1. The detailed derivations and relevant parameter settings are given in the Appendix A.

B. Coupled NCPD using APG and low-rank approximation

In CoNCPD-APG algorithm, the time-consumption of updating $\mathcal{D}^{(s)}$ and $\mathbf{U}^{(n,s)}$ is mainly attributed to the multiplication of $(\mathbf{U}^{(s)})^\circledast \operatorname{vec}(\mathcal{M}^{(s)})$ and $\mathcal{M}_{(n)}^{(s)} \mathbf{U}^{(s)\circledast-n}$ in (10) and (13), and it will be increasingly serious especially for the tensors with large dimensionality. Specifically, in each iteration, let $R^{(s)} = R$, the computational complexity of $(\mathbf{U}^{(s)})^\circledast \operatorname{vec}(\mathcal{M}^{(s)})$ reaches $\mathcal{O}(SR \prod_n I_n)$ and $\mathcal{M}_{(n)}^{(s)} \mathbf{U}^{(s)\circledast-n}$ has the complexity of $\mathcal{O}(NSR \prod_n I_n)$. The applications of low-rank approximation in nonnegative matrix/tensor factorization have demonstrated their performance improvement in terms of computational efficiency while maintaining computational accuracy [34, 35, 43]. Generally, the unconstrained CPD of a tensor converges in dozens of iterations and is considered faster than its counterpart with nonnegative constraint. Therefore, to reduce the

Algorithm 1: CoNCPD-APG algorithm

Input: $\mathcal{M}^{(s)}$, L_n and $R^{(s)}$, $n=1, \dots, N$, $s=1, \dots, S$

- 1 Initialization:
- 2 $\mathbf{U}^{(n,s)}$, $\mathcal{D}^{(s)}$, $\mathcal{M}_{(n)}^{(s)}$, $n=1, \dots, N$, $s=1, \dots, S$
- 3 **for** $k=1, 2, \dots, \text{MaxIt}$ **do**
- 4 **for** $s=1, \dots, S$ **do**
- 5 Calculate $\hat{\mathcal{G}}_{k-1}^{(s)}$ and $\hat{\mathcal{D}}_{k-1}^{(s)}$ via (10) and (16)
- 6 Update $\mathcal{D}_k^{(s)}$ via (9)
- 7 **end**
- 8 **for** $n=1, 2, \dots, N$ **do**
- 9 **for** $s=1, \dots, S$ **do**
- 10 Calculate $\hat{\mathbf{G}}_{k-1}^{(n,s)}$ and $\hat{\mathbf{U}}_{k-1}^{(n,s)}$ via (13) and (17)
- 11 Update $\mathbf{U}_k^{(n,s)}$ via (12), (14) and (15)
- 12 **end**
- 13 **end**
- 14 **if** $F(k) \geq F(k-1)$ **then**
- 15 $\hat{\mathcal{D}}_{k-1}^{(s)} = \mathcal{D}_{k-1}^{(s)}$, $\hat{\mathbf{U}}_{k-1}^{(n,s)} = \mathbf{U}_{k-1}^{(n,s)}$
- 16 Reupdate $\mathcal{D}_k^{(s)}$, $\mathbf{U}_k^{(n,s)}$ via (9), (12), (14) and (15)
- 17 **end**
- 18 **if** *stopping criterion is satisfied* **then**
- 19 **return**
- 20 $\mathbf{U}_k^{(n,s)}$, $\mathcal{D}_k^{(s)}$, $n=1, \dots, N$, $s=1, \dots, S$
- 21 **end**
- 22 **end**

Output: $\mathbf{U}^{(n,s)}$, $\mathcal{D}^{(s)}$, $n=1, \dots, N$, $s=1, \dots, S$

computational complexity of CoNCPD-APG algorithm, we consider introducing the low-rank approximation of $\mathcal{M}^{(s)}$ before performing the actual coupled decomposition. Suppose that $\left[\tilde{\mathbf{U}}^{(1,s)}, \tilde{\mathbf{U}}^{(2,s)}, \dots, \tilde{\mathbf{U}}^{(N,s)} \right]$ is the rank- $\tilde{R}^{(s)}$ approximation of $\mathcal{M}^{(s)}$ obtained by the unconstrained CPD, $\tilde{\mathbf{U}}^{(n,s)} \in \mathbb{R}^{I_n \times \tilde{R}^{(s)}}$, $\tilde{R}^{(s)} \leq R^{(s)}$, thus the cost function in (7) can be represented as the optimization problem in (18) (see it at the top of next page) with fixed $\tilde{\mathbf{U}}^{(1,s)}, \tilde{\mathbf{U}}^{(2,s)}, \dots, \tilde{\mathbf{U}}^{(N,s)}$. In other words, instead of loading the original tensor $\mathcal{M}^{(s)}$ directly into the iterations, we first split the tensor into smaller compressed matrices, such as $\tilde{\mathbf{U}}^{(1,s)}, \tilde{\mathbf{U}}^{(2,s)}, \dots, \tilde{\mathbf{U}}^{(N,s)}$, and then bring them into the decomposition iterations, which can greatly reduce the time and space complexities of algorithms[34]. Via low-rank approximation, $\operatorname{vec}(\mathcal{M}^{(s)})$ and $\mathcal{M}_{(n)}^{(s)}$ in (10) and (13) can be respectively expressed by $\operatorname{vec}(\mathcal{M}^{(s)}) = \tilde{\mathbf{U}}^{(s)\circledast} \operatorname{ddiag}(\mathcal{I})$ and

$\mathcal{M}_{(n)}^{(s)} = \tilde{U}^{(s,n)} (\tilde{U}^{(s)\circ-n})^T$, and $\mathcal{I} \in \mathbb{R}^{\tilde{R}^{(s)} \times \dots \times \tilde{R}^{(s)}}$ denotes a core tensor with all super-diagonal elements being 1. This thereby leads to

$$\begin{aligned} \left(\mathbf{U}^{(s)\circ} \right)^T \text{vec} \left(\mathcal{M}^{(s)} \right) &= \left(\mathbf{U}^{(s)\circ} \right)^T \tilde{U}^{(s)\circ} \text{ddiag}(\mathcal{I}) \\ &= \left(\mathbf{U}^{(s)T} \tilde{U}^{(s)} \right)^{\otimes} \text{ddiag}(\mathcal{I}) \end{aligned} \quad (19)$$

and

$$\begin{aligned} \mathcal{M}_{(n)}^{(s)} \mathbf{U}^{(s)\circ-n} &= \tilde{U}^{(s,n)} \left(\tilde{U}^{(s)\circ-n} \right)^T \mathbf{U}^{(s)\circ-n} \\ &= \tilde{U}^{(s,n)} \left(\tilde{U}^{(s)T} \mathbf{U}^{(s)} \right)^{\otimes-n}. \end{aligned} \quad (20)$$

By virtue of low-rank approximation, only very small matrices are involved to perform the multiplications in (20) and (19). In addition, the computational complexities of $(\mathbf{U}^{(s)\circ})^T \text{vec}(\mathcal{M}^{(s)})$ and $\mathcal{M}_{(n)}^{(s)} \mathbf{U}^{(s)\circ-n}$ are respectively reduced to $\mathcal{O}(SR\tilde{R} \sum_n I_n)$ and $\mathcal{O}(NSR\tilde{R} \sum_n I_n)$ via the transformation of (19) and (20) (here we set $\tilde{R}^{(s)} = \tilde{R}$).

Overall, to develop an efficient coupled tensor decomposition algorithm, we further propose the IraCoNCPD-APG algorithm based on CoNCPD-APG algorithm and low-rank approximation. The implementation of IraCoNCPD-APG algorithm includes two steps: (i) performing unconstrained CPD of tensors $\mathcal{M}^{(s)}$ successively to achieve their low-rank approximation as $\mathcal{M}^{(s)} \approx \left[\tilde{U}^{(1,s)}, \tilde{U}^{(2,s)}, \dots, \tilde{U}^{(N,s)} \right]$; (ii) updating $\mathbf{U}_k^{(n,s)}$ and $\mathcal{D}_k^{(s)}$ via solving the optimization problem in (18) with fixed $\tilde{U}^{(1,s)}, \tilde{U}^{(2,s)}, \dots, \tilde{U}^{(N,s)}$. The framework of IraCoNCPD-APG algorithm is presented in Algorithm 2.

Algorithm 2: larCoNCPD-APG algorithm

Input: $\mathcal{M}^{(s)}$, L_n , and $R^{(s)}$, $n = 1, \dots, N$,
 $s = 1, \dots, S$

- 1 Initialization:
- 2 $\mathbf{U}^{(n,s)}$, $\mathcal{D}^{(s)}$, $\mathcal{M}_{(n)}^{(s)}$, $n = 1, \dots, N$, $s = 1, \dots, S$
- 3 Calculate $\tilde{U}^{(n,s)}$, $n = 1, \dots, N$, $s = 1, \dots, S$ via unconstrained CPD on $\mathcal{M}^{(s)}$, $s = 1, \dots, S$
- 4 **for** $k = 1, 2, \dots, \text{MaxIt}$ **do**
- 5 Repeat the 4th to 21st command lines of Algorithm 1 except the 5th and 10th lines:
- 6 Calculate $\hat{\mathcal{G}}_{k-1}^{(s)}$ and $\hat{\mathcal{G}}_{k-1}^{(n,s)}$ via (10) and (13) by introducing (19) and (20)
- 7 **end**

Output: $\mathbf{U}^{(n,s)}$, $\mathcal{D}^{(s)}$, $n = 1, \dots, N$, $s = 1, \dots, S$

C. Remarks and discussion

1) *Acceleration strategy:* Even though we have introduced low-rank approximation to reduce the computation load of CoNCPD-APG algorithm, there is still some way to speed up the algorithm. In conventional NCPD problem, core tensor \mathcal{D} is generally merged into the factor matrices that can reduce the computation load to a certain extent. Analogously, this strategy can be extended to the coupled NCPD problem, but only for the cases where all N modes are not fully coupled between

tensors [11], e.g., $\exists n, L_n = 0$. However, for the cases of $\forall n, L_n > 0$, the core tensors $\mathcal{D}^{(s)}$ are required and defined to differentiate the magnitude of corresponding components (rank-1 tensor) between tensors. In *Experiment 1*, we design the coupled NCPD problem using synthetic data and verify the importance of core tensors in some cases. In *Experiment 3*, the scaling features of corresponding brain activities provided by core tensors extracted from ERP tensors are used to classify the groups of patients and healthy controls. Therefore, this acceleration strategy depends on the coupling constraints of tensor data.

2) *Computational complexity:* In this study, for the computational complexity, we mainly refer to the time complexity based on the multiplication operations. From Section III, we can note that the main computational load is dominated by the updates of $\mathcal{D}^{(s)}$ and $\mathbf{U}^{(n,s)}$, especially the calculation of block-partial gradients $\tilde{\mathcal{G}}^{(s)}$ and $\tilde{\mathcal{G}}^{(n,s)}$ in (10) and (13). The specific costs of calculating them (n th mode of s th tensor) are listed in Table II. Let $\tilde{R}^{(s)} = R$, taking into consideration that there are N modes and S tensors, the total time complexity for each iteration of CoNCPD-APG algorithm reaches $\mathcal{O}(NSR \prod_{n=1}^N I_n)$. By introducing low-rank approximation, (10) and (13) can be calculated using (19) and (20), the costs of which are also given in Table II. Let $\tilde{R}^{(s)} = R$, the overall computation load per iteration of IraCoNCPD-APG algorithm is reduced to $\mathcal{O}(NSR^2 \sum_{n=1}^N I_n)$.

3) *Termination criteria:* In this study, we consider two iteration termination parameters: the change of relative error (RelErr) and the maximum number of iterations (MaxIt). We define

$$\text{RelErr} \triangleq \frac{1}{S} \sum_{s=1}^S \left[\|\mathcal{M}^{(s)} - \hat{\mathcal{M}}^{(s)}\|_F / \|\mathcal{M}^{(s)}\|_F \right] \quad (21)$$

where $\mathcal{M}^{(s)}$ and $\hat{\mathcal{M}}^{(s)}$ are the original and recovered tensors. Furthermore, we stipulate $|\text{RelErr}_{\text{new}} - \text{RelErr}_{\text{old}}| < \varepsilon$, i.e., the adjacent RelErr change should be smaller than the preselected threshold. In this study, we choose $\varepsilon = 1e-8$ and MaxIt=1000 in CoNCPD algorithms, and $\varepsilon = 1e-4$ and MaxIt=200 in unconstrained CPD algorithm.

4) *Model Order Selection:* In terms of the number of components and coupled components, i.e., $R^{(s)}$, $s = 1, 2, \dots, S$ and L_n , $n = 1, 2, \dots, N$, we set ground-truth values for the synthetic data. For the real-world data, we adopt the principal component analysis (PCA) method to calculate the number of components, and the number of principal components with 99% explained variance is selected as the number of components; we adopt the correlation analysis to calculate the number of coupled components, for example, if components of different groups have a fairly high correlation coefficient, such as 0.8, we consider them to be coupled components. For the number of components $\tilde{R}^{(s)}$ in low-rank approximation, we use the DIFFIT method.

IV. EXPERIMENTS

In this section, aiming to examine and demonstrate the superior performance of CoNCPD-APG and IraCoNCPD-APG algorithms on coupled NCPD problem, we design and

$$\begin{aligned}
 \min_{\mathcal{D}^{(s)}, \mathbf{U}^{(n,s)}} \mathcal{F} & \frac{1}{2} \sum_{s=1}^S \left\| \left[\tilde{\mathbf{U}}^{(1,s)}, \tilde{\mathbf{U}}^{(2,s)}, \dots, \tilde{\mathbf{U}}^{(N,s)} \right] - \left[\mathcal{D}^{(s)}; \mathbf{U}^{(1,s)}, \mathbf{U}^{(2,s)}, \dots, \mathbf{U}^{(N,s)} \right] \right\|_F^2 \\
 \text{s.t. } \mathcal{D}^{(s)} & \in \mathbb{R}_+^{I_1 \times \dots \times I_N}, \mathbf{U}^{(n,s)} \in \mathbb{R}_+^{I_n \times R^{(s)}}, \tilde{\mathbf{U}}^{(n,s)} \in \mathbb{R}^{I_n \times \tilde{R}^{(s)}}, \tilde{R}^{(s)} \leq R^{(s)}
 \end{aligned} \tag{18}$$

TABLE II
TIME COMPLEXITY PER ITERATION IN CoNCPD-APG AND IraCoNCPD-APG ALGORITHMS: n TH MODE OF s TH TENSOR

Equation	Operation	Description	Input size	Output size	Cost
(10)	① = $(\mathbf{U}^{(s)T} \mathbf{U}^{(s)})^\circledast$	Hadamard product	$I_n \times R, n = 1, 2, \dots, N$	$R \times R$	$R^2 \sum_{n=1}^N I_n + R^2 N$
(10)	② = $(\mathbf{U}^{(s)\circledast})^T$	Khatri-Rao product	$I_n \times R, n = 1, 2, \dots, N$	$R \times \prod_{n=1}^N I_n$	$R \prod_{n=1}^N I_n$
(10)	③ = ② · $\text{vec}(\mathcal{M}^{(s)})$	Matrix product	$R \times \prod_{n=1}^N I_n, \prod_{n=1}^N I_n \times 1$	$R \times 1$	$R \prod_{n=1}^N I_n$
(13)	④ = $(\mathbf{U}^{(s)T} \mathbf{U}^{(s)})^{\circledast-n}$	Hadamard product	$I_m \times R, m = 1, \dots, N, m \neq n$	$R \times R$	$R^2 \sum_{m \neq n}^N I_m + R^2(N-1)$
(13)	⑤ = $\tilde{\mathbf{U}}^{(n,s)} \cdot \textcircled{4}$	Matrix product	$I_n \times R, R \times R$	$I_n \times R$	$R^2 I_n$
(13)	⑥ = $\mathbf{U}^{(s)\circledast-n}$	Khatri-Rao product	$I_m \times R, m = 1, \dots, N, m \neq n$	$\prod_{m \neq n}^N I_m \times R$	$R \prod_{m \neq n}^N I_m$
(13)	⑦ = $\mathcal{M}^{(s)} \cdot \textcircled{6}$	Matrix product	$I_n \times \prod_{m \neq n}^N I_m, \prod_{m \neq n}^N I_m \times R$	$I_n \times R$	$R \prod_{n=1}^N I_n$
(19)	⑧ = $(\mathbf{U}^{(s)T} \tilde{\mathbf{U}}^{(s)})^\circledast$	Hadamard product	$I_n \times R, n = 1, 2, \dots, N$	$R \times R$	$R^2 \sum_{n=1}^N I_n + R^2 N$
(20)	⑨ = $(\tilde{\mathbf{U}}^{(s)T} \mathbf{U}^{(s)})^{\circledast-n}$	Hadamard product	$I_m \times R, m = 1, \dots, N, m \neq n$	$R \times R$	$R^2 \sum_{m \neq n}^N I_m + R^2(N-1)$
(20)	⑩ = $\tilde{\mathbf{U}}^{(s,n)} \cdot \textcircled{9}$	Matrix product	$I_n \times R, R \times R$	$I_n \times R$	$R^2 I_n$

¹ Here let $R^{(s)} = \tilde{R}^{(s)} = R, s = 1, 2, \dots, S$.

perform three experiments on synthetic data, face image data and real-world electroencephalography (EEG) data. We adopt alternating least squares (ALS, [4]) algorithm to implement the low-rank approximation, which has proven to be a reasonable solver for unconstrained CPD problems [35]. The optimization strategies including fast hierarchical alternating least squares (fHALS, [27, 28, 44]), multiplicative updating (MU, [45, 46]) and ALS are used as the competitors to the proposed algorithms. Additionally, we also introduce the low-rank approximation to fHALS-based algorithm.

For algorithm performance comparison, we adopt decomposition quality indicators including RelErr, objective function value (ObjFun), tensor fitting value (TenFit) and performance index (PI), as well as execution time (Time). TenFit $\triangleq \frac{1}{S} \sum_{s=1}^S \left[1 - \|\mathcal{M}^{(s)} - \hat{\mathcal{M}}^{(s)}\|_F / \|\mathcal{M}^{(s)}\|_F \right]$, and it is used to present the fittings between original and recovered tensors. PI is used to evaluate the recovery accuracy of factor matrices and defined as

$$\begin{aligned}
 \text{FacFit} \triangleq & \frac{1}{2R(R-1)} \left[\sum_{i=1}^R \left(\sum_{j=1}^R \frac{|g_{ij}|}{\max_k |g_{ik}|} \right) \right. \\
 & \left. + \sum_{i=1}^R \left(\sum_{j=1}^R \frac{|g_{ji}|}{\max_k |g_{ki}|} \right) \right] \tag{22}
 \end{aligned}$$

where g_{ij} denotes the (i, j) th element of $\mathbf{G} = (\bar{\mathbf{U}})^\dagger \mathbf{U}$. $\bar{\mathbf{U}}$ is the recovered estimation of factor matrix \mathbf{U} and \dagger denotes the pseudo inverse operator. The small value of PI indicates an accurate estimation of the true factor matrix. The input factor matrices and core tensors are initialized with uniformly distributed pseudorandom numbers generated by matlab function `rand`. Signal-to-noise ratio (SNR) is defined as $\text{SNR} = 10 \log_{10}(p_s/p_n)$, where p_s and p_n denote signal level and noise level, respectively.

The experiments are carried out with the following computer configurations: CPU-Intel Core i5-7500 @3.40Hz; Memory-16.00 Gb; System-64-bit Windows 10; Software-matlab R2016b.

Experiment 1 Synthetic data. In this part, we design an experiment to illustrate the performance of CoNCPD-APG and IraCoNCPD-APG algorithms in terms of decomposition efficiency and accuracy using synthetic data, and compare them with or without core tensors during the optimization process. Here the algorithms without optimizing core tensors are respectively termed as CoNCPD-APG-NC and IraCoNCPD-APG-NC. We construct 10 third-order tensors partially coupled in three modes according to equation (6) and set the size of tensors to $I_1 = 8n, I_2 = 9n$ and $I_3 = 10n$, where n ranges from 2 to 12. The number of components and coupled components of tensors are set to $R^{(s)} = \text{round}(I_2/2)$ and $L_{1,2,3} = \text{round}(I_2/4)$, and `round` is a matlab function that towards nearest integer. The performance curves including PI, Tenfit, Time and ObjFun versus the size of tensors are illustrated in Figure 1 with contributions from 50 independent runs under the SNR of 20dB.

From Figure 1, we can see that CoNCPD-APG achieves the best decomposition accuracy in terms of PI, Tenfit and ObjFun, followed by IraCoNCPD-APG, CoNCPD-APG-NC and IraCoNCPD-APG-NC. However, CoNCPD-APG is the most time-consuming, followed by CoNCPD-APG-NC and then by IraCoNCPD-APG and IraCoNCPD-APG-NC. The introduction of low-rank approximation can greatly reduce the execution time, and this advantage becomes more significant as the size of tensors increases. Meanwhile, its cost is only a slight reduction in decomposition accuracy. Since the core tensors are not updated in the optimization process, the time consumption of CoNCPD-APG-NC is also alleviated, but the decomposition accuracy of CoNCPD-APG-NC and

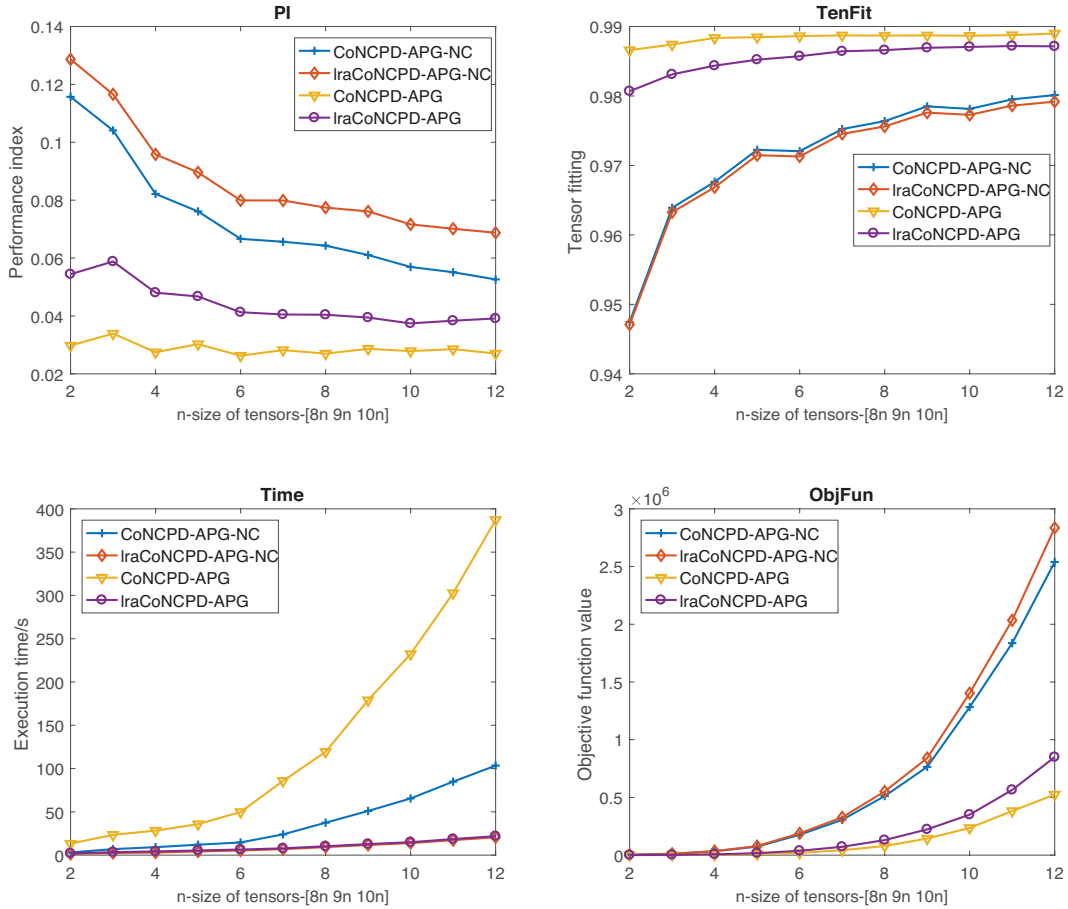


Fig. 1. PI, Tenfit, Time and ObjFun curves of all compared algorithms versus the size of tensors under SNR=20dB and 50 independent runs.

IraCoNCPD-APG-NC is reduced to some extent.

Experiment 2 Face image data. In this experiment, we use the extended Yale B face database¹ for coupled tensor decomposition analysis via image reconstruction and denoising. This database contains gray-scale face images of 38 subjects obtained under 9 poses and 64 illumination conditions [47]. For this database, we only use the cropped images under frontal pose of all illuminations² [48]. Each subject corresponds to 64 images, and each cropped image is resized to 32×32 pixels. Finally, we construct 31 third-order tensors by stacking corresponding face images of each subject along illumination conditions, and the size of each tensor is 32 pixels × 32 pixels × 64 conditions (Data of 7 subjects were not used because of incompleteness).

In terms of the number of components for each tensor, a simple explained variance-based method is adopted in this study. Through unfolding along the first mode, each tensor can be reconstructed into a matrix with the size of 32×2048. Then performing principle component analysis (PCA) on the matrices successively, and the number of principle components with a total explained variance of 99% is regarded as the corresponding component number. Using this method, the component number of tensors for 31 subjects are separately

TABLE III
PERFORMANCE COMPARISON OF IMAGE RECONSTRUCTION AND DENOISING ON YALE B FACE DATABASE BASED ON COUPLED NCPD MODEL (WITH 0.1 SALT&PEPPER NOISE)

Methods	ALS	fHALS	lra&fHALS	APG	lra&APG
RelErr	18.37	15.92	15.98	15.56	15.59
TenFit	0.4075	0.4866	0.4844	0.4980	0.4971
ObjFun	3.80e9	2.81e9	2.84e9	2.68e9	2.69e9
Time	101.50	94.59	19.84	95.53	12.58
PNSR	16.02	19.93	19.78	20.80	20.73

TABLE IV
PERFORMANCE COMPARISON OF IMAGE RECONSTRUCTION AND DENOISING ON YALE B FACE DATABASE BASED ON COUPLED NCPD MODEL (WITH 0.0001 SALT&PEPPER NOISE)

Methods	ALS	fHALS	lra&fHALS	APG	lra&APG
RelErr	13.68	8.96	9.08	7.61	7.65
TenFit	0.5587	0.7108	0.7071	0.7544	0.7531
ObjFun	1.74e9	7.25e8	7.43e8	5.07e8	5.12e8
Time	103.84	96.34	20.59	87.70	12.51
PNSR	16.51	20.16	20.03	21.52	21.47

¹<http://vision.ucsd.edu/~leekc/ExtYaleDatabase/ExtYaleB.html>

²<http://www.cad.zju.edu.cn/home/dengcai/Data/FaceData.html>

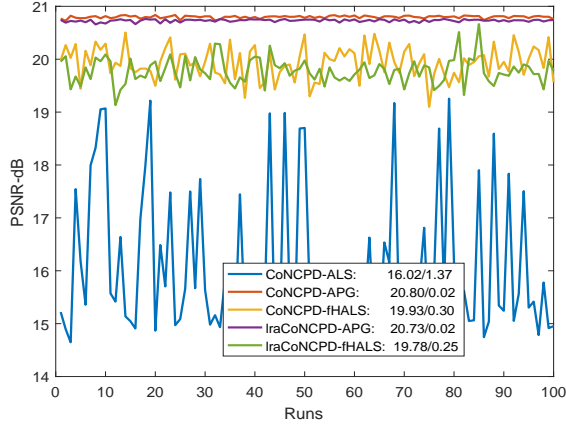


Fig. 2. PSNR values of all compared algorithms for image reconstruction and denoising with 0.1 salt-and-pepper noise over 100 independent runs based on coupled NCPD model and their means and standard deviations (SDs)

selected. In this experiment, we assume that the coupling information between tensors exists in their three modes, and totally 20 coupled components among tensors were extracted.

We compare CoNCPD-APG and IraCoNCPD-APG algorithms with their competitors on two noisy image datasets of 0.1 and 0.0001 salt-and-pepper noise. The value of peak-signal-to-noise ratio (PSNR) is also used to measure the quality of reconstructed face images. Table III and IV give the algorithm performance comparison averaged from 100 independent runs under two noise settings. From the tables, we can see that the proposed APG-based algorithms are superior to other algorithms, as they obtain lower RelErr and ObjFun values, as well as higher tensor fittings and PSNRs. It indicates that the proposed algorithms have higher decomposition accuracy and stronger image reconstruction capabilities. More importantly, by introducing low-rank approximation strategy, IraCoNCPD-APG and IraCoNCPD-fHALS algorithms can greatly reduce execution time while maintaining decomposition performance. It should be noted that the execution time of Ira-based algorithms showed in tables includes the running time of the unconstrained CPD and the running time of APG/fHALS optimization in the CoNCPD problem. In addition, Figure 2 illustrates the PSNR value curves of all the compared algorithms over 100 independent runs, indicating that the proposed CoNCPD-APG and IraCoNCPD-APG algorithms have excellent decomposition stability compared with competitors.

Experiment 3 Real-world ERP data. In this experiment, we compare the proposed CoNCPD-APG and IraCoNCPD-APG algorithms with CoNCPD-MU, CoNCPD-fHALS and IraCoNCPD-fHALS algorithms in the multi-domain feature extraction of event-related potential (ERP) data³ (ALS-based algorithm is excluded due to its poor performance). Two groups of data are chosen: 21 children with reading disability (RD) and 21 children with attention deficit (AD), aiming to acquire multi-domain features of ERP data which can better discriminate the two groups. Using complex Morlet

TABLE V
PERFORMANCE COMPARISON OF THE ALGORITHMS IN MULTI-DOMAIN FEATURE EXTRACTION OF ERP DATA BASED ON COUPLED NCPD MODEL

Methods	MU	fHALS	Ira&fHALS	APG	Ira&APG
RelErr	6.83	7.06	7.02	6.34	6.34
TenFit	0.8373	0.8319	0.8327	0.8490	0.8490
ObjFun	6.34e5	6.87e5	6.81e5	5.48	5.47e5
Time	164.30	192.71	39.35	183.91	27.45
MCC-Mean	0.7293	0.8782	0.8621	0.8896	0.8916
MCC-SD	0.1770	0.0973	0.1171	0.0956	0.0809

wavelet transform, we generate the third-order tensors of 42 subjects (21 RD & 21 AD) with the size of 9 (channels) \times 71 (frequency bins) \times 60 (temporal points) to testify the effectiveness and practicality of coupled tensor decomposition. Following [49], we set the number of components to $R^{(1)} = R^{(2)} = \dots R^{(42)} = 36$. Considering the nature of ERP data, we assume that these third-order ERP tensors are coupled in spatial, spectral and temporal modes, and we directly set the number of coupled components to 36.

ERP data are acquired through repeated presentation of stimuli, which makes their properties in temporal, spectral and spatial domains roughly known before they are actually extracted. According to prior knowledge given in [49], we can select the expected multi-domain features and their corresponding temporal, spectral and spatial components from the decomposition results of ERP data. Figure 3 gives an example illustration of multi-domain features and their corresponding components extracted by CoNCPD-APG algorithm in the 1st run. For multi-domain feature shown in the figure, statistical analysis using t-test reveals the significant difference between RD and AD groups with $t_{20} = 2.419$, $p = 0.025$. The relevant temporal component (latency peaks around 150 ms) and spectral component (spectrum peaks around 5 Hz) closely match the property of mismatch negativity component [49]. The corresponding topography denotes that the difference of RD and AD groups may appear in the central and left hemisphere [49].

We adopt three steps to verify the stability of multi-domain feature extraction of all the compared algorithms in 100 runs. (1) We select the multi-domain features and their parallel three components in the 1st runs of 5 algorithms. (2) We average the selected ones separately as a set of template patterns, which are termed as \mathbf{u}_{temp}^{fea} , \mathbf{u}_{temp}^{tem} , \mathbf{u}_{temp}^{spe} and \mathbf{u}_{temp}^{spa} . (3) We define the maximum correlation coefficient (MCC) between template patterns and feature-based components of k th runs as follows

$$MCC(k) = \max [\text{corr}(\mathbf{u}_{temp}^{fea}, \mathbf{U}_k^{fea}) \otimes \text{corr}(\mathbf{u}_{temp}^{tem}, \mathbf{U}_k^{tem}) \otimes \text{corr}(\mathbf{u}_{temp}^{spe}, \mathbf{U}_k^{spe}) \otimes \text{corr}(\mathbf{u}_{temp}^{spa}, \mathbf{U}_k^{spa})] \quad (23)$$

where k denotes the run number and `corr` is a matlab function which returns a vector containing the pairwise linear correlation coefficient between \mathbf{u} and \mathbf{U} . \mathbf{U}_k^{fea} , \mathbf{U}_k^{tem} , \mathbf{U}_k^{spe} and \mathbf{U}_k^{spa} represent multi-domain features and their corresponding temporal, spectral and spatial components in the k th run, respectively. Obviously, if the MCC is close to 1, it means that the extraction of multi-domain features is more stable.

³http://www.escience.cn/people/cong/AdvancedSP_ERP.html

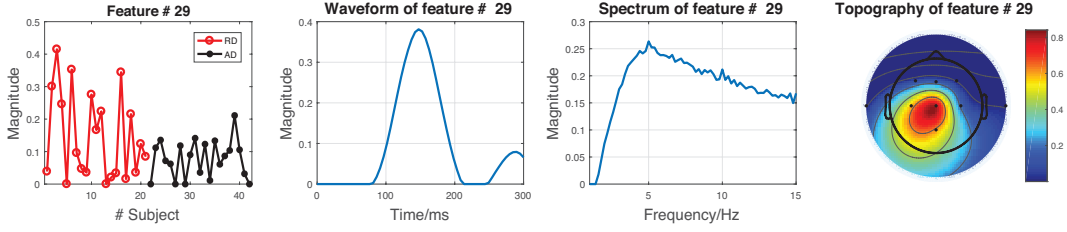


Fig. 3. An example of multi-domain feature and its related temporal, spectral and spatial components of ERP data extracted by CoNCPD-APG algorithm

Table V gives the average RelErr, ObjFun, TenFit and Time from 100 independent runs for ERP data, as well as the means and SDs of MCCs of multi-domain features. From the table, we see that the proposed CoNCPD-APG and lraCoNCPD-APG algorithms are superior to competitors in terms of decomposition accuracy and multi-domain feature extraction stability. Interestingly, the MU-based couple method achieves better performance than the fHALS-based algorithms in accuracy but has the worst multi-domain feature extraction stability. This experiment also proves that the low-rank approximation in coupling analysis of large-scale tensors can greatly improve computation efficiency without losing the decomposition accuracy.

V. CONCLUSION

In this study, we considered the coupled tensor decomposition problem, aiming to solve the simultaneous decomposition of nonnegative multi-block tensors. To improve convergence speed and optimization accuracy, we first proposed a coupled nonnegative CANDECOMP/PARAFAC decomposition algorithm based as alternating proximal gradient (APG) method (CoNCPD-APG). Then by combining APG and low-rank approximation, we further proposed the lraCoNCPD-APG algorithm. We also gave some discussions on the properties of the proposed algorithms as well as some implementation remarks. Experiments of synthetic data, real-world face image data and event-related potential (ERP) data were conducted to compare the proposed algorithms with fast hierarchical alternating least squares (fHALS), multiplicative updating (MU) and alternating least squares (ALS)-based algorithms in the designed coupled NCPD problems. The experiment results illustrated that the proposed algorithms are superior to competitors in terms of decomposition accuracy, image reconstruction capability and multi-domain feature extraction stability, and also demonstrated that the introduction of low-rank approximation can greatly improve the computation efficiency without compromising the decomposition quality. Determining the number of coupled components depends on the validity of potential assumptions and relevant prior knowledge. So far, its selection in real-world applications is still subjective to a certain extent, which remains it an open issue and will be one of our future works.

APPENDIX A

For completeness of this paper, in this section, some steps of algorithm derivations and relevant parameter settings will be further explained below.

A. CoNCPD-APG algorithm

Following [39, 41], by using Lagrange multiplier method, we obtain (9), (12), (14) and (15) from (8) and (11). When updating the core tensor $\mathcal{D}^{(s)}$, by keeping all factor matrices $\mathbf{U}^{(n,s)}$ fixed, we first convert (7) to

$$F_d = \frac{1}{2} \left\| \text{vec}(\mathcal{M}^{(s)}) - \mathbf{U}^{(s)\odot} \text{ddiag}(\mathcal{D}^{(s)}) \right\|_F^2 \quad (24)$$

where $\text{vec}(\mathcal{M}^{(s)})$ denotes the vectorization of tensor $\mathcal{M}^{(s)}$. Mathematically, the squared Frobenius norm of a matrix can be replaced by the trace of multiplication of the matrix and its transpose. Then (24) can be represented as:

$$F_d = \frac{1}{2} \text{tr} \left[\left(\text{vec}(\mathcal{M}^{(s)}) - \mathbf{U}^{(s)\odot} \text{ddiag}(\mathcal{D}^{(s)}) \right)^T \left(\text{vec}(\mathcal{M}^{(s)}) - \mathbf{U}^{(s)\odot} \text{ddiag}(\mathcal{D}^{(s)}) \right) \right] \quad (25)$$

According to trace property, the block-partial gradient $\hat{\mathcal{G}}^{(s)}$ of (25) with respect to $\hat{\mathcal{D}}^{(s)}$ can be calculated by

$$\begin{aligned} \hat{\mathcal{G}}^{(s)} &= \nabla_{\hat{\mathcal{D}}^{(s)}} F_d \\ &= \text{ddiag} \left[\left(\mathbf{U}^{(s)\odot} \right)^T \mathbf{U}^{(s)\odot} \text{ddiag} \left(\hat{\mathcal{D}}^{(s)} \right) \right] \\ &\quad - \text{ddiag} \left[\left(\mathbf{U}^{(s)\odot} \right)^T \text{vec} \left(\mathcal{M}^{(s)} \right) \right] \end{aligned} \quad (26)$$

where the outer notation ‘ddiag’ means the tensorization from a vector to a super-diagonal tensor, which is the reverse operation of inner one. Using the property of Khatri-Rao product, we can efficiently calculate $(\mathbf{U}^{(s)\odot})^T \mathbf{U}^{(s)\odot}$ by

$$\left(\mathbf{U}^{(s)\odot} \right)^T \mathbf{U}^{(s)\odot} = \left(\mathbf{U}^{(s)T} \mathbf{U}^{(s)} \right)^{\otimes} \quad (27)$$

When updating the factor matrix (without coupling information) $\mathbf{U}^{(n,s)}$, by keeping all other variables $\mathbf{U}^{(m,s)}$, $m \neq n$ and $\mathcal{D}^{(s)}$ fixed, (7) is represented as follows:

$$F_u = \frac{1}{2} \left\| \mathcal{M}_{(n)}^{(s)} - \mathbf{U}^{(n,s)} \mathcal{D}^{(s)} \left(\mathbf{U}^{(s)\odot -n} \right)^T \right\|_F^2 \quad (28)$$

where $\mathcal{M}_{(n)}^{(s)}$ denotes the mode- n matricization of $\mathcal{M}^{(s)}$. $\mathcal{D}^{(s)}$ is a diagonal matrix and its diagonal elements correspond to the super-diagonal elements of core tensor $\mathcal{D}^{(s)}$. Similarly,

the block-partial gradient $\hat{\mathbf{G}}^{(n,s)}$ of (28) at $\hat{\mathbf{U}}^{(n,s)}$ can be calculated as:

$$\begin{aligned}\hat{\mathbf{G}}^{(n,s)} &= \nabla_{\hat{\mathbf{U}}^{(n,s)}} F_u \\ &= \hat{\mathbf{U}}^{(n,s)} \mathbf{D}^{(s)} \left(\mathbf{U}^{(s)\odot-n} \right)^T \mathbf{U}^{(s)\odot-n} \left(\mathbf{D}^{(s)} \right)^T \\ &\quad - \mathcal{M}_{(n)}^{(s)} \mathbf{U}^{(s)\odot-n} \left(\mathbf{D}^{(s)} \right)^T \\ &= \hat{\mathbf{U}}^{(n,s)} \mathbf{D}^{(s)} \left(\mathbf{U}^{(s)T} \mathbf{U}^{(s)} \right)^{\otimes-n} \mathbf{D}^{(s)} \\ &\quad - \mathcal{M}_{(n)}^{(s)} \mathbf{U}^{(s)\odot-n} \mathbf{D}^{(s)}\end{aligned}\quad (29)$$

However, when updating the factor matrix $\mathbf{U}^{(n,s)}$ which consists of two parts: $\mathbf{U}_C^{(n,s)}$ and $\mathbf{U}_I^{(n,s)}$, we first substitute $\mathbf{U}^{(n,s)} = \begin{bmatrix} \mathbf{U}_C^{(n,s)} & \mathbf{U}_I^{(n,s)} \end{bmatrix}$ into (28) and have

$$F_{ci} = \frac{1}{2} \left\| \mathcal{M}_{(n)}^{(s)} - \begin{bmatrix} \mathbf{U}_C^{(n,s)} & \mathbf{U}_I^{(n,s)} \end{bmatrix} \mathbf{D}^{(s)} \left(\mathbf{U}^{(s)\odot-n} \right)^T \right\|_F^2 \quad (30)$$

Let $\mathbf{B}^{(n,s)} = \mathbf{D}^{(s)} \left(\mathbf{U}^{(s)\odot-n} \right)^T \in \mathbb{R}_+^{R^{(s)} \times \prod_{m \neq n}^N I_m}$. Let $\hat{\mathbf{G}}_C^{(n,s)}$ denote the block-partial gradient of (30) at $\hat{\mathbf{U}}_C^{(n,s)}$, which can be calculated as:

$$\begin{aligned}\hat{\mathbf{G}}_C^{(n,s)} &= \nabla_{\hat{\mathbf{U}}_C^{(n,s)}} F_{ci} \\ &= \hat{\mathbf{U}}_C^{(n,s)} \mathbf{B}_C^{(n,s)} \left(\mathbf{B}_C^{(n,s)} \right)^T \\ &\quad - \left(\mathcal{M}_{(n)}^{(s)} - \hat{\mathbf{U}}_I^{(n,s)} \mathbf{B}_I^{(n,s)} \right) \left(\mathbf{B}_C^{(n,s)} \right)^T \\ &= \left(\hat{\mathbf{U}}_C^{(n,s)} \mathbf{B}_C^{(n,s)} - \mathcal{M}_{(n)}^{(s)} \right) \left(\mathbf{B}_C^{(n,s)} \right)^T\end{aligned}\quad (31)$$

where $\hat{\mathbf{U}}_C^{(n,s)}$ denotes an extrapolated point of $\mathbf{U}_C^{(n,s)}$. $\mathbf{B}^{(n,s)} = \begin{bmatrix} \mathbf{B}_C^{(n,s)}; \mathbf{B}_I^{(n,s)} \end{bmatrix}$, $\mathbf{B}_C^{(n,s)} \in \mathbb{R}_+^{L_n \times \prod_{m \neq n}^N I_m}$ and $\mathbf{B}_I^{(n,s)} \in \mathbb{R}_+^{(R^{(s)}-L_n) \times \prod_{m \neq n}^N I_m}$. From (29) and (31), it can be inferred that $\hat{\mathbf{G}}_C^{(n,s)}$ is equal to $\hat{\mathbf{G}}_{:,1:L_n}^{(n,s)}$. Analogously, the block-partial gradient $\hat{\mathbf{G}}_I^{(n,s)}$ at $\hat{\mathbf{U}}_I^{(n,s)}$ can be obtained as $\hat{\mathbf{G}}_{:,L_n:R^{(s)}}^{(n,s)}$ and $\hat{\mathbf{G}}^{(n,s)} = \begin{bmatrix} \hat{\mathbf{G}}_C^{(n,s)} & \hat{\mathbf{G}}_I^{(n,s)} \end{bmatrix}$.

B. Parameter settings

Consider updating $\mathcal{D}^{(s)}$ and $\mathbf{U}^{(n,s)}$ at the k th iteration. Following [-], we set the Lipschitz constants $L_{d,k-1}^{(s)}$ and $L_{u,k-1}^{(n,s)}$ as:

$$L_{d,k-1}^{(s)} = \left\| \left(\mathbf{U}_{k-1}^{(s)\odot} \right)^T \mathbf{U}_{k-1}^{(s)\odot} \right\| \quad (32)$$

and

$$L_{u,k-1}^{(n,s)} = \left\| \mathbf{D}_{k-1}^{(s)} \left(\mathbf{U}_{k-1}^{(s)\odot-n} \right)^T \mathbf{U}_{k-1}^{(s)\odot-n} \mathbf{D}_{k-1}^{(s)} \right\| \quad (33)$$

where $\|\cdot\|$ denotes the spectral norm. Using the property of Khatri-Rao product, we can also efficiently calculate $L_{d,k-1}^{(s)}$ and $L_{u,k-1}^{(n,s)}$ through

$$\begin{aligned}\left(\mathbf{U}_{k-1}^{(s)\odot} \right)^T \mathbf{U}_{k-1}^{(s)\odot} &= \left[\left(\mathbf{U}_{k-1}^{(n,s)} \right)^T \mathbf{U}_{k-1}^{(n,s)} \right]^{\otimes} \\ \left(\mathbf{U}_{k-1}^{(s)\odot-n} \right)^T \mathbf{U}_{k-1}^{(s)\odot-n} &= \left[\left(\mathbf{U}_{k-1}^{(m,s)} \right)^T \mathbf{U}_{k-1}^{(m,s)} \right]^{\otimes-n}\end{aligned}\quad (34)$$

We take the extrapolation weights as

$$w_{d,k-1}^{(s)} = \min \left(\hat{w}_{k-1}, \delta_w \sqrt{\frac{L_{d,k-2}^{(s)}}{L_{d,k-1}^{(s)}}} \right) \quad (35)$$

and

$$w_{u,k-1}^{(n,s)} = \min \left(\hat{w}_{k-1}, \delta_w \sqrt{\frac{L_{u,k-2}^{(n,s)}}{L_{u,k-1}^{(n,s)}}} \right) \quad (36)$$

where $\delta_w < 1$ is predefined (e.g., 0.9999, [42]), and $\hat{w}_{k-1} = \frac{t_{k-1}-1}{t_k}$ with $t_0 = 1$ and $t_k = \frac{1}{2} \left(1 + \sqrt{1 + 4t_{k-1}^2} \right)$. Moreover, we define the extrapolation at points $\mathcal{D}_{k-1}^{(s)}$ and $\mathbf{U}_{k-1}^{(n,s)}$ as

$$\hat{\mathcal{D}}_{k-1}^{(s)} = \mathcal{D}_{k-1}^{(s)} + w_{d,k-1}^{(s)} \left(\mathcal{D}_{k-1}^{(s)} - \mathcal{D}_{k-2}^{(s)} \right) \quad (37)$$

and

$$\hat{\mathbf{U}}_{k-1}^{(n,s)} = \mathbf{U}_{k-1}^{(n,s)} + w_{u,k-1}^{(n,s)} \left(\mathbf{U}_{k-1}^{(n,s)} - \mathbf{U}_{k-2}^{(n,s)} \right) \quad (38)$$

ACKNOWLEDGMENT

This work is supported by National Natural Science Foundation of China (Grant No.91748105), National Foundation in China (No. JCKY2019110B009 & 2020-JCJQ-JJ-252), the Fundamental Research Funds for the Central Universities [DUT2019& DUT20LAB303] in Dalian University of Technology in China. This study is to memorize Prof. Tapani Ristaniemi for his great help to the authors, Fengyu Cong and Xiulin Wang.

REFERENCES

- [1] F. L. Hitchcock, "The expression of a tensor or a polyadic as a sum of products," *Journal of Mathematics and Physics*, vol. 6, no. 1-4, pp. 164–189, 1927.
- [2] R. A. Harshman *et al.*, "Foundations of the parafac procedure: Models and conditions for an" explanatory" multimodal factor analysis," 1970.
- [3] J. D. Carroll and J.-J. Chang, "Analysis of individual differences in multidimensional scaling via an n-way generalization of "eckart-young" decomposition," *Psychometrika*, vol. 35, no. 3, pp. 283–319, 1970.
- [4] A. Cichocki, R. Zdunek, A. H. Phan, and S.-i. Amari, *Nonnegative matrix and tensor factorizations: applications to exploratory multi-way data analysis and blind source separation*. John Wiley & Sons, 2009.
- [5] F. Cong, Q.-H. Lin, L.-D. Kuang, X.-F. Gong, P. Astikainen, and T. Ristaniemi, "Tensor decomposition of eeg signals: a brief review," *Journal of neuroscience methods*, vol. 248, pp. 59–69, 2015.
- [6] F. Cong, A.-H. Phan, P. Astikainen, Q. Zhao, Q. Wu, J. K. Hietanen, T. Ristaniemi, and A. Cichocki, "Multi-domain feature extraction for small event-related potentials through nonnegative multi-way array decomposition from low dense array eeg," *International journal of neural systems*, vol. 23, no. 02, p. 1350006, 2013.
- [7] T. G. Kolda and B. W. Bader, "Tensor decompositions and applications," *SIAM review*, vol. 51, no. 3, pp. 455–500, 2009.

- [8] A. Cichocki, D. Mandic, L. De Lathauwer, G. Zhou, Q. Zhao, C. Caiafa, and H. A. Phan, "Tensor decompositions for signal processing applications: From two-way to multiway component analysis," *IEEE signal processing magazine*, vol. 32, no. 2, pp. 145–163, 2015.
- [9] N. D. Sidiropoulos, L. De Lathauwer, X. Fu, K. Huang, E. E. Papalexakis, and C. Faloutsos, "Tensor decomposition for signal processing and machine learning," *IEEE Transactions on Signal Processing*, vol. 65, no. 13, pp. 3551–3582, 2017.
- [10] G. Zhou, Q. Zhao, Y. Zhang, T. Adali, S. Xie, and A. Cichocki, "Linked component analysis from matrices to high-order tensors: Applications to biomedical data," *Proceedings of the IEEE*, vol. 104, no. 2, pp. 310–331, 2016.
- [11] X. Wang, W. Liu, P. Toivainen, T. Ristaniemi, and F. Cong, "Group analysis of ongoing eeg data based on fast double-coupled nonnegative tensor decomposition," *Journal of neuroscience methods*, vol. 330, p. 108502, 2020.
- [12] Y. Jonmohamadi, S. Muthukumaraswamy, J. Chen, J. Roberts, R. Crawford, and A. Pandey, "Extraction of common task features in eeg-fmri data using coupled tensor-tensor decomposition," *bioRxiv*, p. 685941, 2019.
- [13] X.-F. Gong, Q.-H. Lin, F.-Y. Cong, and L. De Lathauwer, "Double coupled canonical polyadic decomposition for joint blind source separation," *IEEE Transactions on Signal Processing*, vol. 66, no. 13, pp. 3475–3490, 2018.
- [14] M. Sørensen, I. Domanov, and L. De Lathauwer, "Coupled canonical polyadic decompositions and (coupled) decompositions in multilinear rank- $(l_r, n, l_r, n, 1)$ terms—part ii: Algorithms," *SIAM Journal on Matrix Analysis and Applications*, vol. 36, no. 3, pp. 1015–1045, 2015.
- [15] B. Hunyadi, P. Dupont, W. Van Paesschen, and S. Van Huffel, "Tensor decompositions and data fusion in epileptic electroencephalography and functional magnetic resonance imaging data," *Wiley Interdisciplinary Reviews: Data Mining and Knowledge Discovery*, vol. 7, no. 1, p. e1197, 2017.
- [16] Z. Xue, S. Yang, H. Zhang, and P. Du, "Coupled higher-order tensor factorization for hyperspectral and lidar data fusion and classification," *Remote Sensing*, vol. 11, no. 17, p. 1959, 2019.
- [17] A. Cichocki, "Tensor decompositions: a new concept in brain data analysis?" *arXiv preprint arXiv:1305.0395*, 2013.
- [18] V. D. Calhoun, J. Liu, and T. Adali, "A review of group ica for fmri data and ica for joint inference of imaging, genetic, and erp data," *Neuroimage*, vol. 45, no. 1, pp. S163–S172, 2009.
- [19] X.-F. Gong, X.-L. Wang, and Q.-H. Lin, "Generalized non-orthogonal joint diagonalization with lu decomposition and successive rotations," *IEEE Transactions on Signal Processing*, vol. 63, no. 5, pp. 1322–1334, 2015.
- [20] M. Mørup, "Applications of tensor (multiway array) factorizations and decompositions in data mining," *Wiley Interdisciplinary Reviews: Data Mining and Knowledge Discovery*, vol. 1, no. 1, pp. 24–40, 2011.
- [21] T. Yokota, A. Cichocki, and Y. Yamashita, "Linked parafac/cp tensor decomposition and its fast implementation for multi-block tensor analysis," in *International Conference on Neural Information Processing*. Springer, 2012, pp. 84–91.
- [22] X. Wang, C. Zhang, T. Ristaniemi, and F. Cong, "Generalization of linked canonical polyadic tensor decomposition for group analysis," in *International Symposium on Neural Networks*. Springer, 2019, pp. 180–189.
- [23] G. Zhou, A. Cichocki, Y. Zhang, and D. P. Mandic, "Group component analysis for multiblock data: Common and individual feature extraction," *IEEE transactions on neural networks and learning systems*, vol. 27, no. 11, pp. 2426–2439, 2015.
- [24] E. Acar, Y. Levin-Schwartz, V. D. Calhoun, and T. Adali, "Tensor-based fusion of eeg and fmri to understand neurological changes in schizophrenia," in *2017 IEEE International Symposium on Circuits and Systems (ISCAS)*. IEEE, 2017, pp. 1–4.
- [25] E. Karahan, P. A. Rojas-Lopez, M. L. Bringas-Vega, P. A. Valdes-Hernandez, and P. A. Valdes-Sosa, "Tensor analysis and fusion of multimodal brain images," *Proceedings of the IEEE*, vol. 103, no. 9, pp. 1531–1559, 2015.
- [26] C. Chatzichristos, M. Davies, J. Escudero, E. Kofidis, and S. Theodoridis, "Fusion of eeg and fmri via soft coupled tensor decompositions," in *2018 26th European Signal Processing Conference (EUSIPCO)*. IEEE, 2018, pp. 56–60.
- [27] X. Wang, T. Ristaniemi, and F. Cong, "Fast implementation of double-coupled nonnegative canonical polyadic decomposition," in *ICASSP 2019-2019 IEEE International Conference on Acoustics, Speech and Signal Processing (ICASSP)*. IEEE, 2019, pp. 8588–8592.
- [28] R. Zdunek, K. Fonał, and A. Wołczowski, "Linked cp tensor decomposition algorithms for shared and individual feature extraction," *Signal Processing: Image Communication*, vol. 73, pp. 37–52, 2019.
- [29] C. I. Kanatsoulis, X. Fu, N. D. Sidiropoulos, and W.-K. Ma, "Hyperspectral super-resolution: A coupled tensor factorization approach," *IEEE Transactions on Signal Processing*, vol. 66, no. 24, pp. 6503–6517, 2018.
- [30] S. Li, R. Dian, L. Fang, and J. M. Bioucas-Dias, "Fusing hyperspectral and multispectral images via coupled sparse tensor factorization," *IEEE Transactions on Image Processing*, vol. 27, no. 8, pp. 4118–4130, 2018.
- [31] M. Sørensen and L. De Lathauwer, "Coupled tensor decompositions for applications in array signal processing," in *2013 5th IEEE International Workshop on Computational Advances in Multi-Sensor Adaptive Processing (CAMSAP)*. IEEE, 2013, pp. 228–231.
- [32] B. Ermiş, E. Acar, and A. T. Cemgil, "Link prediction in heterogeneous data via generalized coupled tensor factorization," *Data Mining and Knowledge Discovery*, vol. 29, no. 1, pp. 203–236, 2015.
- [33] E. Acar, R. Bro, and A. K. Smilde, "Data fusion in metabolomics using coupled matrix and tensor factorizations," *Proceedings of the IEEE*, vol. 103, no. 9, pp. 1602–1620, 2015.

- [34] G. Zhou, A. Cichocki, and S. Xie, "Fast nonnegative matrix/tensor factorization based on low-rank approximation," *IEEE Transactions on Signal Processing*, vol. 60, no. 6, pp. 2928–2940, 2012.
- [35] Y. Zhang, G. Zhou, Q. Zhao, A. Cichocki, and X. Wang, "Fast nonnegative tensor factorization based on accelerated proximal gradient and low-rank approximation," *Neurocomputing*, vol. 198, pp. 148–154, 2016.
- [36] N. Parikh, S. Boyd *et al.*, "Proximal algorithms," *Foundations and Trends® in Optimization*, vol. 1, no. 3, pp. 127–239, 2014.
- [37] Y. E. Nesterov, "A method for solving the convex programming problem with convergence rate $o(1/k^2)$," in *Dokl. akad. nauk Sssr*, vol. 269, 1983, pp. 543–547.
- [38] A. Beck and M. Teboulle, "A fast iterative shrinkage-thresholding algorithm for linear inverse problems," *SIAM journal on imaging sciences*, vol. 2, no. 1, pp. 183–202, 2009.
- [39] N. Guan, D. Tao, Z. Luo, and B. Yuan, "Nenmf: An optimal gradient method for nonnegative matrix factorization," *IEEE Transactions on Signal Processing*, vol. 60, no. 6, pp. 2882–2898, 2012.
- [40] D. Wang, Y. Zhu, T. Ristaniemi, and F. Cong, "Extracting multi-mode erp features using fifth-order nonnegative tensor decomposition," *Journal of neuroscience methods*, vol. 308, pp. 240–247, 2018.
- [41] Y. Xu and W. Yin, "A block coordinate descent method for regularized multiconvex optimization with applications to nonnegative tensor factorization and completion," *SIAM Journal on imaging sciences*, vol. 6, no. 3, pp. 1758–1789, 2013.
- [42] Y. Xu, "Alternating proximal gradient method for sparse nonnegative tucker decomposition," *Mathematical Programming Computation*, vol. 7, no. 1, pp. 39–70, 2015.
- [43] F. Cong, G. Zhou, P. Astikainen, Q. Zhao, Q. Wu, A. K. Nandi, J. K. Hietanen, T. Ristaniemi, and A. Cichocki, "Low-rank approximation based non-negative multi-way array decomposition on event-related potentials," *International journal of neural systems*, vol. 24, no. 08, p. 1440005, 2014.
- [44] A. Cichocki and A.-H. Phan, "Fast local algorithms for large scale nonnegative matrix and tensor factorizations," *IEICE transactions on fundamentals of electronics, communications and computer sciences*, vol. 92, no. 3, pp. 708–721, 2009.
- [45] D. D. Lee and H. S. Seung, "Learning the parts of objects by non-negative matrix factorization," *Nature*, vol. 401, no. 6755, p. 788, 1999.
- [46] H. Lee and S. Choi, "Group nonnegative matrix factorization for EEG classification," in *Artificial Intelligence and Statistics*, 2009, pp. 320–327.
- [47] A. S. Georghiades, P. N. Belhumeur, and D. J. Kriegman, "From few to many: Illumination cone models for face recognition under variable lighting and pose," *IEEE transactions on pattern analysis and machine intelligence*, vol. 23, no. 6, pp. 643–660, 2001.
- [48] D. Cai, X. He, and J. Han, "Spectral regression for efficient regularized subspace learning," in *2007 IEEE 11th international conference on computer vision*. IEEE, 2007, pp. 1–8.
- [49] F. Cong, A. H. Phan, Q. Zhao, T. Huttunen-Scott, J. Kaartinen, T. Ristaniemi, H. Lyytinen, and A. Cichocki, "Benefits of multi-domain feature of mismatch negativity extracted by non-negative tensor factorization from eeg collected by low-density array," *International journal of neural systems*, vol. 22, no. 06, p. 1250025, 2012.